Chemomechanical Origin of Hydrogen Trapping at Grain Boundaries in fcc Metals

Xiao Zhou,[1] Daniel Marchand,[1] David L. McDowell,[2] Ting Zhu,[2] and Jun Song[1,*]
[1]Department of Mining and Materials Engineering, McGill University, Montréal, Québec H3A 0C5, Canada
[2]Woodruff School of Mechanical Engineering, Georgia Institute of Technology, Atlanta, Georgia 30332, USA
(Received 2 November 2015; published 19 February 2016)

Hydrogen embrittlement of metals is widely observed, but its atomistic origins remain little understood and much debated. Combining a unique identification of interstitial sites through polyhedral tessellation and first-principles calculations, we study hydrogen adsorption at grain boundaries in a variety of face-centered cubic metals of Ni, Cu, γ-Fe, and Pd. We discover the chemomechanical origin of the variation of adsorption energetics for interstitial hydrogen at grain boundaries. A general chemomechanical formula is established to provide accurate assessments of hydrogen trapping and segregation energetics at grain boundaries, and it also offers direct explanations for certain experimental observations. The present study deepens our mechanistic understanding of the role of grain boundaries in hydrogen embrittlement and points to a viable path towards predictive microstructure engineering against hydrogen embrittlement in structural metals.

DOI: 10.1103/PhysRevLett.116.075502

Despite drastic technological advances in the development of polymers and composites in the past several decades, metals remain the irreplaceable backbone in many important applications for the automotive, aerospace, and energy industries. However, metals are typically susceptible to environmental attack. One prominent example is hydrogen embrittlement (HE) that can result in sudden and catastrophic failure of metallic components and systems [1]. Hydrogen is abundant in service environments and manufacturing processes. As a result, HE poses a significant threat to load-bearing metallic components and is often considered as a major obstacle to the reliable applications of structural metals. Despite considerable effort in the study of HE [2–15], the dominant physical mechanisms of HE remain controversial [16,17]. Hence, the study of HE at the atomistic and electronic levels may illuminate the mechanistic origin of HE and thus enable the development of an effective means to mitigate HE. Moreover, the influence of hydrogen on dislocation migration can be distinguished from its role in grain boundary (GB) segregation and compromise of fracture resistance. We focus on the latter here.

Hydrogen adsorption is favored at microstructural heterogeneities [18], such as GBs, as opposed to in interstitial sites in the bulk lattice. Recently, Bechtle *et al.* [19] conducted experiments on GB-engineered Ni samples with and without hydrogen, and their results showed that the susceptibility of HE can be drastically redued at special GBs that are characterized with low excess free volumes and a high degree of atomic matching. In addition, Oudriss *et al.* [20] showed that special GBs can trap hydrogen and reduce hydrogen diffusion. These studies highlight the important role of GBs in influencing hydrogen transport and embrittlement behaviors and suggest the possibility of controlling the susceptibility of structural metals to HE through GB engineering.

To advance rational GB engineering, it is essential to characterize the GBs and associated hydrogen segregation behaviors in a systematic and quantitative manner. The structure of certain high angle tilt GBs is commonly described by the coincidence site lattice (CSL) model [21]. Alternatively, the GB structure can be represented by a periodic array of nested three-dimensional (3D) structural units [22,23], which are associated with CSL boundaries but also pertain to general high angle tilt grain boundaries. Along this line of approach, Ashby, Spaepen, and Williams [24] showed that there exist eight unique convex polyhedrons with triangle faces (i.e., so-called deltahedra) to account for all possible basic packing units at a tilt GB. This approach enables the characterization of GBs with a simple, yet powerful, concept of a geometric packing unit, which can be applied to investigate many structural and chemomechanical properties of GBs, such as interstitial impurity segregation at GBs [25,26].

Here we develop a novel modeling approach that combines the space tessellation of polyhedral packing units and first-principles density functional theory (DFT) calculations for studying the hydrogen segregation at GBs in structural metals. Using several face-centered cubic (fcc) metals, including Ni, Cu, γ-Fe, and Pd as representative systems, we demonstrate that the polyhedral packing units at GBs can be uniquely identified and their central holes are shown to serve as favorable interstitial sites of hydrogen adsorption. Our DFT calculations reveal a universal dependence of hydrogen adsorption energies on the local volume deformation of polyhedral packing units in all four fcc metals studied. To uncover its physical origin, we establish a general formula involving a minimum number of first-principles input and fitting parameters that closely match all DFT data of hydrogen adsorption energies at GBs in four different fcc metals. Such a general result

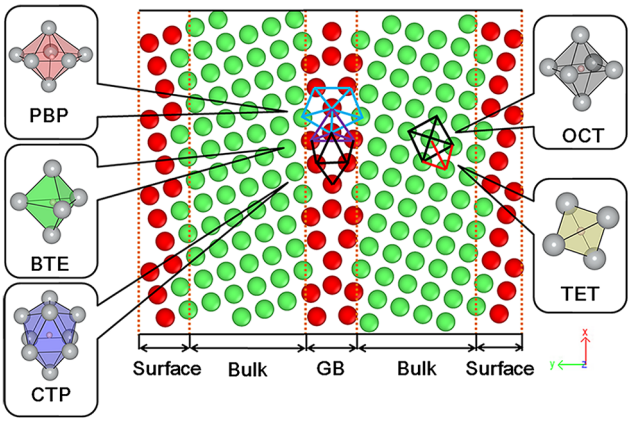

FIG. 1. Schematic illustration of polyhedron in representative $\sum 5(130)[100]$ GB and bulk lattice. The gray ball in the distinguished polyhedron represents the host Ni atom, and the small pink ball in the center is the hydrogen atom.

illuminates the chemomechanical origin of hydrogen segregation at GBs. The physical meaning of the parameters in the formula is clarified. Our results thus provide mechanistic insights towards predictive GB engineering to support the development of HE-resistant metals.

We have studied a number of symmetric tilt GBs with various misorientations in the fcc metals of Ni, Cu, γ-Fe, and Pd. Among these GBs, five types of polyhedrons are involved: i.e., tetrahedron (TET), octahedron (OCT), pentagonal bipyramid (PBP), cap trigonal prism (CTP), and bitetrahedron (BTE) [24], as illustrated in Fig. 1 for a representative $\Sigma 5(130)[100]$ GB [meaning the (130) GB face with a [100] tilt axis] in Ni. We identified these polyhedrons by space tessellation [27]. Energy minimization from DFT calculations indicates that there is only one interstitial site of hydrogen adsorption in each polyhedron, which lies close to the centroid of the polyhedron. This is consistent with the Switendick criterion based on the minimum H-H distance [49]. Hence, the center of each polyhedron corresponds to an individual hydrogen adsorption site at the GBs. In other words, one can identify potential hydrogen adsorption sites along GBs using a geometric approach of space tessellation of polyhedral packing units without a detailed knowledge of hydrogen adsorption chemistry.

After the identification of hydrogen adsorption sites at GBs through space tessellation of polyhedral packing units, we performed DFT calculations to evaluate the interactions between hydrogen and GBs in terms of adsorption energetics. Figure 2 shows the differential charge density of $\Sigma 5(130)[100]$Ni GB projected along the (100) plane (see Fig. S3 for similar plots of other fcc metals studied). These results indicate that the interactions between hydrogen and the host atoms are dominantly localized at GBs, and hence the adsorption energy can be primarily determined by the local environment of the *capsule*, i.e., the polyhedron enclosing the hydrogen atom.

The adsorption energy of hydrogen, E^{ad}, is defined as

$$E^{\mathrm{ad}} = E^{\mathrm{GB}}_{\mathrm{H}} - E^{\mathrm{GB}} - E^{\mathrm{H}}_{\mathrm{iso}}, \quad (1)$$

where E^{GB} and $E^{\mathrm{GB}}_{\mathrm{H}}$ are the total energies of the system before and after adsorption of one hydrogen atom, respectively, and $E^{\mathrm{H}}_{\mathrm{iso}}$ is the energy of one isolated hydrogen atom in vacuum. Based on Eq. (1), we calculated the hydrogen adsorption energies for different polyhedral sites for a series of symmetric tilt GBs [27] in Ni, Cu,γ-Fe, and Pd, as plotted in Fig. 3. Clearly, the hydrogen adsorption energies E^{ad} depend largely on the type of polyhedral interstitial site; i.e., the average values of E^{ad} differ for different types of polyhedra. Moreover, for each type of polyhedral interstitial site, the values of E^{ad} vary markedly. Hence, the polyhedron is not sufficient alone to uniquely determine the interactions between hydrogen and GBs.

To understand the large variation of E^{ad}, we examined the local deformation of polyhedrons at GBs. A parameter, dV_p/V_p^0, is used to measure the local volume changes (dilatation) of polyhedrons. Here, V_p^0 is the volume of the pristine polyhedron, which is defined as the corresponding deltahedron with the edge length being the nearest-neighboring distance, $\sqrt{2}a_0/2$, where a_0 denotes the equilibrium lattice constant in the bulk fcc lattice; furthermore, $dV_p = V_p - V_p^0$ measures the deviation of the actual polyhedron volume V_p from V_p^0. We plot dV_p/V_p^0 together with E^{ad} in Fig. 3. A clear correspondence between the variations in the E^{ad} and dV_p/V_p^0 data can be observed for all four fcc metals studied.

The intriguing correspondence shown in Fig. 3 suggests that the variation of E^{ad} is dictated by the local volume changes of polyhedral packing units. To elucidate the physical origin of such a correspondence, we note that the mechanical interaction energy between a GB and an interstitial point defect can be determined by evaluating the

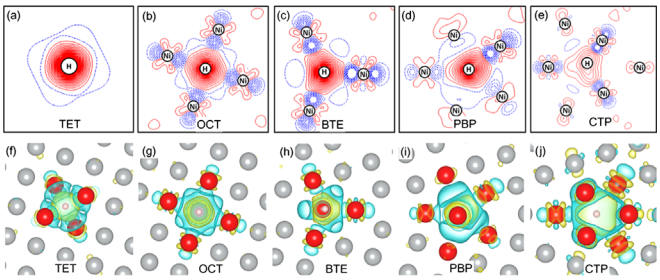

FIG. 2. Differential charge density of $\Sigma 5(130)[100]$Ni GB projected on the (100) plane, with (a)–(e) being two-dimensional while (f)–(j) being three-dimensional charge density contours. In (a)–(e), the blue dashed line represents electron depletion, and the red solid line signifies electron accumulation. In (f)–(j), the red spheres represent Ni atoms locating at the vertices of the polyhedron that encloses the hydrogen atom, indicated by the small pink sphere, while the gray spheres represent other Ni atoms. The blue region represents electron depletion, while the yellow region signifies electron accumulation.

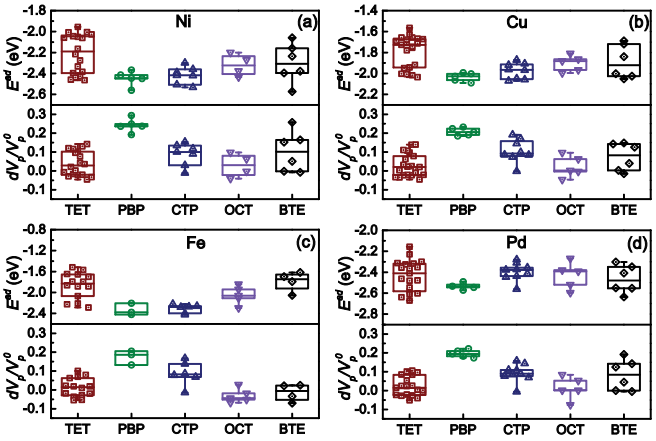

FIG. 3. The variation in the hydrogen adsorption energy E^{ad} and normalized lattice dilatation dV_p/dV_p^0 of polyhedrons in (a) Ni, (b) Cu, (c) γ-Fe, and (d) Pd systems.

work of $P\Omega_p$, which corresponds to the local pressure P in the absence of point defects times the lattice expansion (i.e., partial volume) Ω_p occurring due to the interstitial insertion of a point defect [10,50]. For the present case of hydrogen adsorption at the polyhedral interstitial site, the partial volume Ω_p should be the volume change associated with hydrogen adsorption at the polyhedral interstitial site, and the local pressure P is determined by the volume change dV_p/V_p^0 according to

$$P = -B\frac{dV_p}{V_p^0}, \tag{2}$$

where B is the bulk modulus (see Table I). We note that the bulk modulus of the lattice is an approximation of the local bulk modulus pertaining to GB regions, owing to the differences in atomic coordination and bond lengths, but is used here as a first-order approximation. Consequently, the mechanical interaction energy between the hydrogen and polyhedral packing unit is estimated as

$$dE^{\mathrm{ad}} = -B\Omega_p\frac{dV_p}{V_p^0}. \tag{3}$$

Using Eq. (3), we can express the adsorption energy of a hydrogen atom in a polyhedron packing unit at a GB in terms of

$$E^{\mathrm{ad}} = E_0^{\mathrm{ad}} - B\Omega_p\frac{dV_p}{V_p^0}, \tag{4}$$

where E_0^{ad} is the chemisorption energy of hydrogen in a deltahedron (i.e., a pristine polyhedron as defined earlier). Equation (4) explicitly reveals the dependence of hydrogen adsorption on the chemisorption energy and the mechanical interaction energy, the latter of which is governed by the partial volume of hydrogen insertion and the local volume deformation of the polyhedral structural unit at GBs. In Fig. 4, the fitting curves (dashed lines) based on Eq. (4) overall agree very well with the data points of adsorption energies from DFT calculations. This good agreement also directly explains the correspondence between the variations in the E^{ad} and dV_p/V_p^0 data as observed in Fig. 3. There are, however, noticeable deviations between some of the first-principles data and model predictions in the case of γ-Fe. Such deviations are primarily attributed to our assumption of the isotropic volumetric deformation of polyhedrons in the model [cf. Eq. (4)] while the actual polyhedron distortion can be anisotropic [27]. This suggests the need of a further study to investigate the effect of deformation anisotropy of polyhedrons for improving the model, which will be pursued in the future.

Here for simplicity, yet without loss of generality, we take a single value of partial volume Ω_p for all polyhedrons, given an fcc metal studied [51]. The fitting parameters of E_0^{ad} and Ω_p. are listed in Table I [27].

The close agreement between the DFT data and the predictions based on Eq. (4) shown in Fig. 4 demonstrates that Eq. (4) captures the dominant chemomechanical effects of hydrogen adsorption and segregation at GBs. In Eq. (4), E_0^{ad} can be regarded as an intrinsic property of pristine

TABLE I. List of material properties, i.e., bulk modulus (B), bulk hydrogen partial volume (Ω), predicted hydrogen partial volume at polyhedrons (Ω_p), and model predicted (and DFT calculated) adsorption energy of hydrogen in a pristine polyhedron, i.e., $[\mathrm{Model}]E_0^{\mathrm{ad}}([\mathrm{DFT}]E_0^{\mathrm{ad}})$, in examined material systems.

		System			
Properties		Ni	Cu	γ-Fe	Pd
B (GPa)		195	137	281	168
Ω (Å^3)		2.28	2.68	2.07	2.42
Ω_p (Å^3)		2.03	2.54	1.76	2.19
$[\mathrm{Model}]E_0^{\mathrm{ad}}([\mathrm{DFT}]E_0^{\mathrm{ad}})$ (eV)	TET	−2.11 (−2.06)	−1.72 (−1.72)	−1.82 (−1.87)	−2.38 (−2.35)
	OCT	−2.24 (−2.26)	−1.86 (−1.85)	−2.14 (−2.18)	−2.40 (−2.38)
	BTE	−2.05 (−2.04)	−1.73 (−1.70)	−1.83 (−1.79)	−2.27 (−2.30)
	PBP	−1.85	−1.59	−1.79	−2.06
	CTP	−2.20	−1.75	−2.04	−2.18

polyhedrons associated with the chemisorption of hydrogen, which can be separately determined (other than the GB calculations). The pristine TETs and OCTs are commonly present in a bulk fcc lattice, the pristine BTEs are basic constituents of coherent twin boundaries, and the corresponding hydrogen adsorption energies can be readily evaluated. These data, also listed in Table I, are in close agreement with the E_0^{ad} values obtained from the previous GB calculations. This validates the treatment of E_0^{ad} as a material constant. Incidentally, the pristine PBP and OCT polyhedrons are not present in the GB structures examined in the present study. Nonetheless, we suggest the possible methods (elaborated in details in Ref. [27]) by which one might construct pseudopristine PBP and OCT polyhedrons to compute the corresponding values of E_0^{ad}. In addition, we note that, in Table I, OCT (the polyhedron responsible for H adsorption in bulk lattice) exhibits the lowest E_0^{ad} among all five polyhedrons. Besides, the partial volume of hydrogen adsorption at GBs, Ω_p, is another important parameter in Eq. (4). Interestingly, the value of Ω_p obtained is nearly identical to the partial volume of a hydrogen interstitial in the bulk lattice (see Table I). Hence, hydrogen induces a similar dilatation both at the GB and in the bulk [27].

Equation (4) provides a predictive model for evaluating the energetics of hydrogen trapping and segregation at GBs. It is important to point out that this model is a very general, physics-based model. Besides the fcc metal systems, the model is also expected to be applicable to metals of other crystal structures (e.g., hcp and bcc). Some preliminary calculations have been performed using bcc Nb as an example to demonstrate the generality of the model [27]. In light of recent experiments [19,20,52,53] on hydrogen embrittlement, several case studies of hydrogen embrittlement of GBs were performed, as elaborated in Ref. [27]. Equation (4) enables a quick evaluation of the tendency of hydrogen segregation at GBs. For instance, the

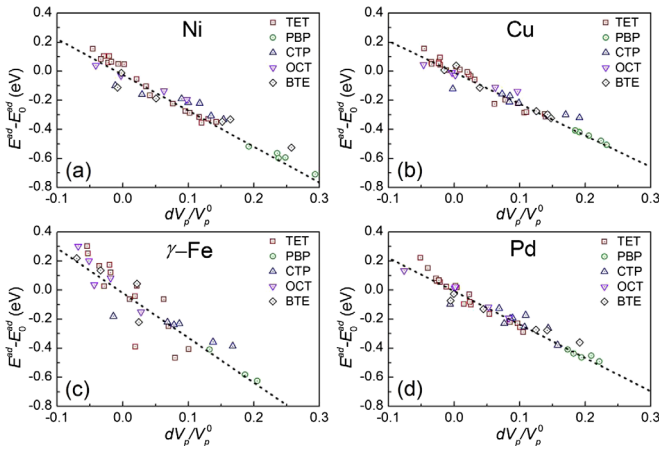

FIG. 4. Comparison between the DFT calculated (open symbols) and model predicted (dashed lines) adsorption energetics versus the volume distortion relation in (a) Ni, (b) Cu, (c) -Fe, and (d) Pd systems.

$\Sigma 3$ and $\Sigma 3^n$ families (i.e., the "special" GBs defined in Ref. [19] and discussed earlier in this paper) and $\Sigma 11$ GB exhibit a lack of volume changes of polyhedral structural units. As a result, they are unfavorable to hydrogen trapping and thus less prone to hydrogen embrittlement in terms of less decrease of work of separation of GBs. In contrast, other GBs with high sigma numbers, such as $\Sigma 17$ and $\Sigma 73$, involve substantial volume changes of polyhedral structural units and are more susceptible to hydrogen trapping and accumulation, thus giving rise to more severe embrittlement effects (see Figs. S8 and S9 in Ref. [27]). This trend is consistent with the experimental observations of hydrogen embrittlement effects on GB-engineered Ni [19], where Ni samples consisting of high-density special boundaries (i.e., principally $\Sigma 3$ twin boundaries) are demonstrated to exhibit good HE resistance.

Moreover, our study suggests a mechanistic pathway for further study of the GB effects on hydrogen embrittlement. First, with polyhedrons as atomic structural units of the metal lattice, the diffusion of hydrogen can be considered as discrete hops between neighboring polyhedra. Given the highly localized interactions between hydrogen and GBs, the jumping trial frequency and migration barrier would presumably depend on the coupling of neighboring polyhedra and their associated dilatation. Recognition of such localized interactions will enable the characterization of the complete diffusion parameters through a finite set of calculations [54], thus greatly facilitating the study of the kinetics of hydrogen migration at GBs. Second, the present study calls for a rigorous continuum micromechanical study on the deformation fields of GBs, e.g., through the generalized Peierls-Nabarro model that treats the atomic interaction right at the GB interface and the continuum elastic interaction for the rest of system [55,56]. This will enable the prediction of volume distortion, dV_p/V_p^0 at GBs directly from continuum micromechanics, and thus reduce the need of intensive first-principles calculations, besides the intrinsic properties of polyhedrons, such as E_0^{ad} and Ω_p. As such, Eq. (4), in conjunction with the aforementioned analyses, would provide a full-scale predictive framework to quantitatively guide the GB engineering against hydrogen embrittlement.

In summary, we study the energetics of hydrogen adsorption for a variety of GB structures by combining the space tessellation of polyhedral packing units and the first-principles calculations. We further develop a physics-based, predictive model, as given by Eq. (4), to reveal the chemomechanical origin of hydrogen trapping and segregation at GBs. This model is validated through the quantitative evaluation of hydrogen adsorption energies as a function of volumetric deformation of polyhedral structural units at GBs for several fcc metals. Our results advance the atomic-level understanding of the role of GBs in hydrogen embrittlement and provide mechanistic insights that may enable predictive GB engineering against hydrogen embrittlement. Such insights can be also fed into

the study of hydrogen adsorption kinetics and fracture mechanics for advancing our understanding of hydrogen-assisted GB decohesion or cracking.

J. S. acknowledges the financial support from McGill Engineering Doctoral Award and National Sciences and Engineering Research Council (NSERC) Discovery grant (Grant No. RGPIN 418469-2012). D. L. M. and T. Z. acknowledge support from QuesTek to study hydrogen effects in metals. X. Z. acknowledges the financial support from China Scholarship Council (CSC). We also acknowledge Supercomputer Consortium Laval UQAM McGill and Eastern Quebec for providing computing power.

*To whom all correspondence should be addressed.
jun.song2@mcgill.ca

[1] W. H. Johnson, Proc. R. Soc. London **23**, 168 (1874).
[2] R. P. Gangloff and R. P. Wei, Metall. Trans. A **8**, 1043 (1977).
[3] J. P. Hirth, Metall. Trans. A **11**, 861 (1980).
[4] I. M. Robertson, Eng. Fract. Mech. **68**, 671 (2001).
[5] M. L. Martin, B. P. Somerday, R. O. Ritchie, P. Sofronis, and I. M. Robertson, Acta Mater. **60**, 2739 (2012).
[6] K. Solanki, M. Tschopp, M. Bhatia, and N. Rhodes, Metall. Mater. Trans. A **44**, 1365 (2013).
[7] S. Wang, M. L. Martin, P. Sofronis, S. Ohnuki, N. Hashimoto, and I. M. Robertson, Acta Mater. **69**, 275 (2014).
[8] S. M. Myers *et al.*, Rev. Mod. Phys. **64**, 559 (1992).
[9] H. Wipf, in *Hydrogen in Metals III Properties and Applications* (Springer, Berlin, 1997), p. 1, online resource.
[10] J. Song and W. A. Curtin, Nat. Mater. **12**, 145 (2013).
[11] S. P. Lynch, Scr. Metall. **13**, 1051 (1979).
[12] S. P. Lynch, Acta Metall. **32**, 79 (1984).
[13] R. Kirchheim, Acta Mater. **55**, 5139 (2007).
[14] R. Kirchheim, Acta Mater. **55**, 5129 (2007).
[15] J. Song and W. A. Curtin, Acta Mater. **59**, 1557 (2011).
[16] G. Lu and E. Kaxiras, Phys. Rev. Lett. **94**, 155501 (2005).
[17] K. Takai, H. Shoda, H. Suzuki, and M. Nagumo, Acta Mater. **56**, 5158 (2008).
[18] A. Pundt and R. Kirchheim, Annu. Rev. Mater. Res. **36**, 555 (2006).
[19] S. Bechtle, M. Kumar, B. P. Somerday, M. E. Launey, and R. O. Ritchie, Acta Mater. **57**, 4148 (2009).
[20] A. Oudriss, J. Creus, J. Bouhattate, C. Savall, B. Peraudeau, and X. Feaugas, Scr. Mater. **66**, 37 (2012).
[21] H. Grimmer, Acta Crystallogr. Sect. A **32**, 783 (1976).
[22] A. Sutton and V. Vitek, Phil. Trans. R. Soc. A **309**, 1 (1983).
[23] A. Sutton and V. Vitek, Phil. Trans. R. Soc. A **309**, 37 (1983).
[24] M. F. Ashby, F. Spaepen, and S. Williams, Acta Metall. **26**, 1647 (1978).
[25] M. I. Baskes and V. Vitek, Metall. Trans. A **16**, 1625 (1985).
[26] M. A. Tschopp, K. N. Solanki, F. Gao, X. Sun, M. A. Khaleel, and M. F. Horstemeyer, Phys. Rev. B **85**, 064108 (2012).
[27] See Supplemental Material at http://link.aps.org/supplemental/10.1103/PhysRevLett.116.075502 a brief discussion of the space tessellation algorithm and additional details, which includes Refs. [28–48].
[28] G. Kresse and J. Furthmüller, Phys. Rev. B **54**, 11169 (1996).
[29] G. Kresse and J. Hafner, Phys. Rev. B **47**, 558 (1993).
[30] P. E. Blöchl, Phys. Rev. B **50**, 17953 (1994).
[31] G. Kresse and D. Joubert, Phys. Rev. B **59**, 1758 (1999).
[32] J. P. Perdew, J. A. Chevary, S. H. Vosko, K. A. Jackson, M. R. Pederson, D. J. Singh, and C. Fiolhais, Phys. Rev. B **46**, 6671 (1992).
[33] J. P. Perdew, K. Burke, and M. Ernzerhof, Phys. Rev. Lett. **77**, 3865 (1996).
[34] V. Lucarini, Symmetry **1**, 21 (2009).
[35] A. Okabe, B. Boots, K. Sugihara, and S. N. Chiu, *Spatial Tessellations: Concepts and Applications of Voronoi Diagrams* (Wiley, New York, 2009), Vol. 501.
[36] G. Schusteritsch and E. Kaxiras, Model. Simul. Mater. Sci. Eng. **20**, 065007 (2012).
[37] Y.-W. You, X.-S. Kong, X.-B. Wu, Y.-C. Xu, Q. F. Fang, J. L. Chen, G.-N. Luo, C. S. Liu, B. C. Pan, and Z. Wang, AIP Adv. **3**, 012118 (2013).
[38] T. Korhonen, M. J. Puska, and R. M. Nieminen, Phys. Rev. B **51**, 9526 (1995).
[39] C. Kittel, P. McEuen, and P. McEuen, *Introduction to Solid State Physics* (Wiley, New York, 1976), Vol. 8.
[40] Y. A. Du, L. Ismer, J. Rogal, T. Hickel, J. Neugebauer, and R. Drautz, Phys. Rev. B **84**, 144121 (2011).
[41] M. J. Mehl and D. A. Papaconstantopoulos, Phys. Rev. B **54**, 4519 (1996).
[42] G. P. M. Leyson, B. Grabowski, and J. Neugebauer, Acta Mater. **89**, 50 (2015).
[43] G. Y. Guo and H. H. Wang, Chin. J. Phys. **38**, 949 (2000).
[44] Y. Fukai, *The Metal-Hydrogen System: Basic Bulk Properties* (Springer, New York, 2006), Vol. 21.
[45] J. E. Angelo, N. R. Moody, and M. I. Baskes, Model. Simul. Mater. Sci. Eng. **3**, 289 (1995).
[46] J. Nocedal and S. J. Wright, Least-Squares Problems in *Numerical Optimization* (Springer, New York, 2006).
[47] K. Robinson, G. Gibbs, and P. Ribbe, Science **172**, 567 (1971).
[48] J. R. Rice and J. S. Wang, Mater. Sci. Eng. A **107**, 23 (1989).
[49] A. C. Switendick, Zeitschrift für Physikalische Chemie **117**, 89 (1979).
[50] J. Friedel, *Dislocations*, Addison-Wesley International Series in the Engineering Sciences (Pergamon, USA edtion distributed by Addison-Wesley, New York, 1964), 1st English edition.
[51] It is worth noting that the partial volume may indeed be slightly different for different polyhedrons. Nonetheless, this simplification should suffice to give a good first-order estimate.
[52] M. Seita, J. P. Hanson, S. Gradečak, and M. J. Demkowicz, Nat. Commun. **6**, 6164 (2015).
[53] V. Randle, Acta Mater. **52**, 4067 (2004).
[54] With the number of unique polyhedrons being eight, there is a finite set of 56 polyhedron couples.
[55] S. Y. Dai, Y. Xiang, and D. J. Srolovitz, Acta Mater. **69**, 162 (2014).
[56] H. Wei, Y. Xiang, and P. B. Ming, Commun. Comput. Phys. **4**, 275 (2008).